ANZIAM J. 59(2018), 313–334
doi:10.1017/S1446181117000396

COUPLE MICROSCALE PERIODIC PATCHES TO SIMULATE MACROSCALE EMERGENT DYNAMICS

HAMMAD ALOTAIBI[1], BARRY COX[1] and A. J. ROBERTS✉[1]

(Received 28 February, 2017; accepted 7 July, 2017; first published online 30 January 2018)

Abstract

Macroscale "continuum" level predictions are made by a new way to construct computationally efficient "wrappers" around fine-scale, microscopic, detailed descriptions of dynamical systems, such as molecular dynamics. It is often significantly easier to code a microscale simulator with periodicity: so the challenge addressed here is to develop a scheme that uses only a given periodic microscale simulator; specifically, one for atomistic dynamics. Numerical simulations show that applying a suitable proportional controller within "action regions" of a patch of atomistic simulation effectively predicts the macroscale transport of heat. Theoretical analysis establishes that such an approach will generally be effective and efficient, and also determines good values for the strength of the proportional controller. This work has the potential to empower systematic analysis and understanding at a macroscopic system level when only a given microscale simulator is available.

2010 *Mathematics subject classification*: primary 37M05; secondary 65P20, 76M28, 91B69.

Keywords and phrases: macroscale dynamics, emergence, periodic microscale, patch scheme, equation-free analysis.

1. Introduction

Computational molecular simulations have become a valuable tool to the point where computation now stands alongside theoretical and experimental methods in addressing problems in materials science. However, the high computational cost often constrains simulations to limited space–time domains [12]. The equation-free multiscale scheme aims to use such microscale molecular simulations to efficiently compute and predict large macroscale space–time dynamics [21, 24]. This article focuses on establishing the basis for a novel design of the equation-free scheme in predicting emergent macroscale properties over large space scales by computing atomistic dynamics only on relatively small widely distributed patches [33]. In the scenario where a user has

[1]School of Mathematical Sciences, University of Adelaide, South Australia, Australia;
e-mail: hammad.alotaibi@adelaide.edu.au, barry.cox@adelaide.edu.au,
anthony.roberts@adelaide.edu.au (http://orcid.org/0000-0001-8930-1552).

coded a microscale simulator with microscale periodicity, our innovation is to show how to couple such small periodic patches, so that the overall scheme predicts the correct macroscale spatial dynamics.

Others have previously used an equation-free approach to aid in molecular simulations [14, 32]. However, they concentrated on issues associated with long-time integration, whereas here we focus upon designing effective algorithms for large space domains. Future development of a full multiscale equation-free scheme would combine both aspects.

Alternative multiscale methods that have been proposed are based upon analogous simulations at the microscale level. For example, in the flow through a porous medium, Hassard et al. [18] used smoothed particle hydrodynamics on the microscale to estimate macroscale volume averaged fluxes, with a view to forming a two-scale model that appears like a finite-volume scheme on the macroscale. For general gradient-driven transport processes, Carr et al. [10] correspondingly proposed an extended distributed microstructure model where the macroscale flux is determined as the average of microscale fluxes within microcells. Both approaches suggest that microscale simulations can be coupled usefully across macroscales. We similarly propose coupling expressed in terms of macroscale quantities (here the temperature). In principle, one or more patches may use the same coupling to couple with surrounding continuum simulations. Thus, our approach may readily form part of a hybrid molecular–continuum method [20].

Section 2 describes our straightforward computational scheme for the simulation of the atoms of a dense gas, listed in supplementary material, Appendix A (supplementary material is available at doi:10.1017/S1446181117000396). Such a scheme is also at the core of more complicated schemes for more complicated molecular simulations [19, 23, 35]. In many scenarios, it is easiest to write a microscale simulator with spatially periodic boundaries: for molecular dynamics some relevant comments by other researchers include "periodic boundaries have been used" [13, p. 248]; "in general, one prefers periodic boundary conditions" [22, p. 260]; and "to circumvent this problem, ... a periodic system may be assumed" [23, p. 477]. One aim of the equation-free approach is to use whatever simulator has been provided and adapt it to macroscale simulations. Hence, the important new challenge we address is to use a triply periodic atomic simulation code as "a given" for the computed patches in an equation-free scheme.

In order to research realistic problems in the future we expect to implement the methodology within one of the established powerful molecular dynamics simulators such as LAMMPS [26]. However, here we focus attention on establishing a proof-of-principle and the fundamental effectiveness of the scheme: for that purpose, our straightforward atomistic code is sufficient.

Our innovation is to couple relatively small, triply periodic, atomistic patches over unsimulated space: the coupling mechanism has to differ from that used in patch schemes to date [24]. Section 3 describes a way to implement a proportional controller [3] in two so-called "action regions" that surround the "core" of each patch.

The average kinetic energy in a core estimates the local temperature in a patch. Then, interpolating such core temperatures over the unsimulated space estimates the macroscale temperature field. The applied control aims to appropriately drive the average kinetic energy in each action region to the corresponding macroscale temperature. Section 5 uses some modern dynamical systems theory [2] to prove that a line of such coupled periodic patches has macroscale dynamics that emerges for a range of initial conditions and for a wide class of microscale systems. Then Section 5.2 explicitly constructs the emergent dynamics for the scheme of controlled patches for a general advection–diffusion partial differential equation (PDE). The construction establishes that there is a good control strength so that the emergent dynamics of the scheme reasonably approximates the correct macroscale advection–diffusion.

Section 4 confirms that the proposed controlled coupling of periodic patches is effective for atomistic simulations, and for a control roughly as predicted by the analysis.

For patch dynamics in space–time, a full implementation involves projective integration forward in time [16, 25, 34]. In such projective integration, the issues of lifting and restriction may become significant computational costs. However, we leave projective integration of periodic patches to future research, and so also leave detailed evidence and discussion on computational savings. Future research could extend the analysis herein to establish the potential for high-order accuracy, in multiple dimensions, analogous to what has been proven for patches with Dirichlet/Neumann/Robin boundaries [30, 31]. Although this article focusses on the macroscale temperature diffusion emerging from an atomistic simulation, the equation-free patch scheme does usefully apply to wave systems [8, 9] and so we expect that controlled periodic patches should also be able to reasonably predict the emergent density–momentum waves of an atomistic simulation.

2. An isolated triply periodic patch

As a first test of our novel methodology, our microscale, detailed simulator is the molecular dynamics of a monatomic gas in three-dimensional (3D) space. The simulator computes the motions of N interacting atoms in a microscale patch of space–time, where for our purposes typically there are up to a few thousand atoms in a patch. For example, Figure 1 shows the apparently chaotic path in space of $N = 64$ atoms in a patch for one short-time simulation. We implemented a triply periodic cubic domain where an atom crossing any face is re-injected into the cube across the opposing face. Our challenge is to develop methods that use such a "given" spatially periodic microscale simulator to predict macroscale dynamics.

As evident in Figure 1, throughout we nondimensionalize all quantities with respect to atomic scales so that, for example, the inter-atomic equilibrium distance is one and the atomic mass is one.

To describe the coded simulator (supplementary material, Appendix A), let $\boldsymbol{x}_i(t)$ denote the position in space of the ith atom as a function of time t and let $\boldsymbol{q}_i(t)$ denote

https://doi.org/10.1017/S1446181117000396 Published online by Cambridge University Press

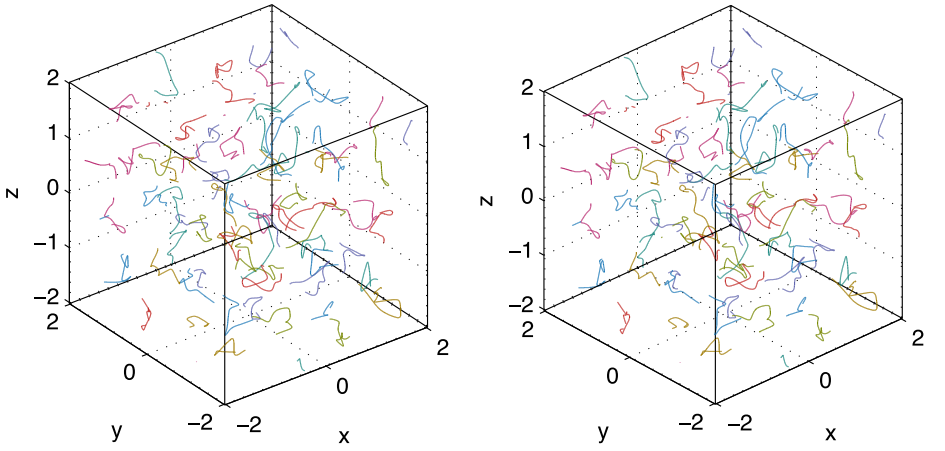

FIGURE 1. Trajectories of 64 atoms, over a time $0 \le t \le 3$, in a triply periodic, cubic, spatial domain, showing the beginnings of the complicated inter-atomic interactions. This stereo pair when viewed cross-eyed gives a 3D effect.

the velocity of the ith atom. Then one set of ordinary differential equations (ODES) for the system are (supplementary material, Appendix A.3, lines 13–16)

$$\frac{d\boldsymbol{x}_i}{dt} = \boldsymbol{q}_i, \quad i = 1, \ldots, N. \tag{2.1}$$

The other set of ODES for the system come from the inter-atomic interactions. For this monatomic gas, we use the classical Lennard-Jones potential (see, for example, [22]) for which the force between atoms separated by a distance r is $F = 1/r^7 - 1/r^{13}$ (nondimensionally). For atoms of nondimensional mass one, Newton's second law then gives the acceleration of each atom as (supplementary material, Appendix A.3, lines 27–35)

$$\frac{d\boldsymbol{q}_i}{dt} = \sum_j \left(\frac{1}{r_{ij}^7} - \frac{1}{r_{ij}^{13}}\right)\frac{\boldsymbol{r}_{ij}}{r_{ij}}, \quad i = 1, \ldots, N, \tag{2.2}$$

where $\boldsymbol{r}_{ij}$ is the displacement vector from the ith atom to the jth, and distance $r_{ij} = |\boldsymbol{r}_{ij}|$. Because the patch is triply periodic, the inter-atomic sum in (2.2) should be over all periodic images of the atoms. Computationally, in the sum we neglect atoms and their images further away than a patch half-width (supplementary material, Appendix A.3, lines 19–24). Due to the $1/r^7$ decay of long-range attraction, and with a typical patch of size $10 \times 10 \times 10$ atoms, the error in accounting for only these atoms/images is roughly $5^{-7} \approx 10^{-5}$—reasonably negligible. Upon checking, the mean momentum is conserved to machine precision, which reflects the symmetry in the coding. Moreover, Figure 2 shows one example of the kinetic and potential energies and their sum; we found that the total energy is typically conserved to a relative error of about 10^{-5}.

Most of the remaining code in the time-derivative routine (supplementary material, Appendix A.3) couples a patch to the macroscale surroundings—described in

https://doi.org/10.1017/S1446181117000396 Published online by Cambridge University Press

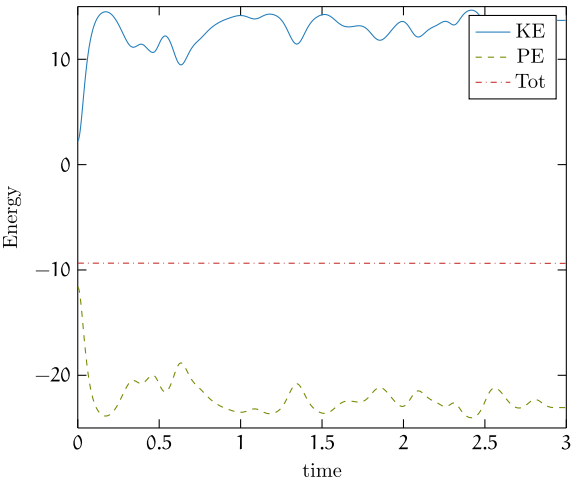

FIGURE 2. For the case of Figure 1, this plot of nondimensional kinetic energy (KE), potential energy (PE), and their sum (Tot) illustrates the conservation of energy by the coded simulation.

Section 3. Our code does not employ any fast multipole or cognate techniques [11], because preliminary exploration indicated that for only a few thousand atoms per patch the fast techniques are not effective. The microscale simulator is then used to integrate the ODES (2.1)–(2.2) in time. For simplicity in this proof-of-principle study, we use a generic MATLAB integration routine (supplementary material, Appendix A.1, line 31) rather than any of the more accurate symplectic integrators that apply to this Hamiltonian system [17, 36]. Such a generic integration routine would not handle the discontinuous re-injection of atoms that leave the cube; consequently, we allow the integrated atom positions to exit the cube smoothly, but map such atoms inside the cubic patch (supplementary material, Appendix A.2) for computing inter-atomic forces and for plotting. Figure 1 plots one very short example simulation with $N = 64$ atoms.

3. Couple patches with a proportional controller

Section 2 described a microscale simulator for the isolated dynamics of atoms in a cubic domain. It is an example of the straightforward code that can be written for simulations which are triply periodic in space. Our innovative challenge is to use the code, as if it were almost a "black box", to simulate over large space–time scales. In our equation-free methodology, such a large-scale space–time simulation is achieved by simulating in small, spatially distributed patches and coupling them over the empty space between the patches [21, 33].

In this first study of the use of periodic patches, we only address the scenario of one large spatial dimension. The other space–time dimensions are assumed small. Further, as a proof-of-principle, this section addresses the specific case of one such periodic

https://doi.org/10.1017/S1446181117000396 Published online by Cambridge University Press

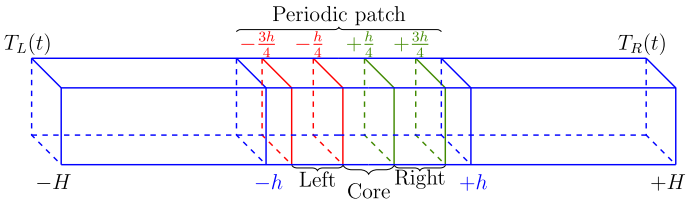

FIGURE 3. The simplest case is one triply periodic patch of atomistic simulation, $-h < x < h$, coupled to distant sidewalls, at $x = \pm H$, of specified temperature. The patch's core region defines its local temperature, and a proportional controller applied in the left and right action regions generates a good macroscale prediction.

patch coupled to "distant" imposed boundary conditions (Section 5 analyses the case of multiple coupled patches in one large dimension). Figure 3 illustrates the scenario with one "small" periodic patch centred on $x = 0$ in a macroscale domain $-H < x < H$. This basic scenario allows us to focus on the key methodological innovation: namely how to couple a microscale periodic patch to the surrounding macroscale environment.

For the purpose of validating our novel patch scheme, in this pilot study we suppose that we want to predict macroscale heat transport by the atomistic simulation. Thus, here we compare the scheme's predictions for the temperature field $T(x, t)$ with the qualitative dynamics of the continuum heat diffusion PDE

$$\frac{\partial T}{\partial t} = K\frac{\partial^2 T}{\partial x^2} \quad \text{such that } T(-H, t) = T_L(t), \quad T(+H, t) = T_R(t). \tag{3.1}$$

Specific initial conditions are not important to our focus on the emergent long-term dynamics.

This section places at the origin a $(2h \times 2h \times 2h)$-periodic patch of the atom simulation, as in Figure 3. This patch extends over $-h < x < h$ within the macroscale domain $-H < x < H$ with specified temperatures, $T_L(t)$ and $T_R(t)$, on the ends of the domain, $x = -H$ and $x = H$, respectively; unsimulated spaces are the comparatively large domains $h < |x| < H$. This article mostly uses the convention of lowercase letters denoting microscale quantities, such as $\boldsymbol{x}$, $\boldsymbol{q}$, and h, and uppercase letters denoting macroscale quantities, such as H and T. Here the problem is assumed to be doubly $2h$-periodic in the other two spatial dimensions; that is, the physical domain is long and thin (Figure 3). We divide the patch into four equal-sized regions (supplementary material, Appendix A.3, lines 38–43):

- the core being $|x| < h/4$ that is used to define macroscale quantities of the patch such as the temperature $T(0, t)$;
- the left action region being $|x + h/2| < h/4$ that is, with the right action region, used to couple the patch to surround macroscale information such as the next patches or the environmental boundary values;
- the right action region being $|x - h/2| < h/4$; and
- a "buffer" region for $|x| > 3h/4$ that caters for a smooth transition between the action regions.

https://doi.org/10.1017/S1446181117000396 Published online by Cambridge University Press

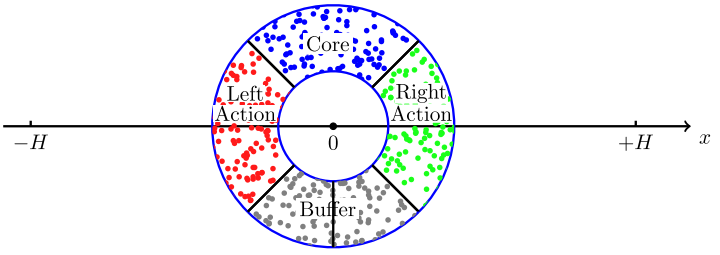

FIGURE 4. A schematic view of a microscale patch that emphasizes the $2h$-periodicity in x and indicating the need for the lower "buffer" region allowing for a smooth transition between the action regions "opposite" the core.

Figure 4 shows an alternative schematic view of the patch; this view emphasizes the microscale $2h$-periodicity in x and the role of the "buffer" region between the two action regions, on the "opposite side" to the important core region.

There appears to be no need for buffer regions between the action regions and the core region [5, 7] (Figures 3 and 4).

We implement a proportional controller [3] to couple the patch to the surrounding macroscale variations (we leave exploration of proportional-integral and proportional-integral-derivative controllers to future research). The applied control is proportional to the differences in the action regions between the macroscale field and the microscale patch simulator. During the atomistic simulation, we compute the nondimensional temperatures in the core and action regions as (supplementary material, Appendix A.3, lines 45–48)

$$T_c = \operatorname*{mean}_{j\in\text{core}} \mathrm{KE}_j, \quad T_l = \operatorname*{mean}_{j\in\text{left}} \mathrm{KE}_j, \quad T_r = \operatorname*{mean}_{j\in\text{right}} \mathrm{KE}_j, \tag{3.2}$$

in terms of the nondimensional kinetic energy of each atom, $\mathrm{KE}_j = |\boldsymbol{q}_j|^2/2$ (the initial conditions and conservation of momentum in the algorithm ensure that the mean velocity of the atoms is zero). With one patch centred at $x = 0$ coupled to boundaries at $x = \pm H$, the scheme's predicted macroscale field for the temperature is the parabolic interpolation through the three values T_L, T_0, and T_R,

$$T(x,t) = T_L\frac{x(x-H)}{2H^2} + T_0\frac{H^2-x^2}{H^2} + T_R\frac{x(x+H)}{2H^2}. \tag{3.3}$$

But, due to the curvature of the parabola, the macroscale core average temperature is slightly different to T_0; averaging (3.3) provides

$$T_c = \frac{2}{h}\int_{-h/4}^{h/4} T(x,t)\,dx = T_0 + \frac{1}{6}\Big(\frac{h}{4H}\Big)^2(T_L - 2T_0 + T_R).$$

Rearranging this identity gives the central temperature

$$T_0 = \frac{T_c - (T_L+T_R)(h/4H)^2/6}{1-(h/4H)^2/3}. \tag{3.4}$$

https://doi.org/10.1017/S1446181117000396 Published online by Cambridge University Press

Then averaging the predicted macroscale field (3.3) over each action region gives that the macroscale interpolation predicts that the action regions should have the average temperatures

$$T_{\text{int},\pm} = T_0 \pm (T_R - T_L)(h/4H) + \tfrac{13}{6}(T_R - 2T_0 + T_L)(h/4H)^2, \tag{3.5}$$

where $\pm$ is for the right/left action region, respectively. The applied control is proportional to the differences between these macroscale predictions (3.5) and the temperatures (3.2) from the patch simulation (supplementary material, Appendix A.3, lines 50–55).

The controller accelerates or decelerates the atoms in the action region accordingly. That is, for each atom, Newton's second law (2.2) is modified by the control to the following (supplementary material, Appendix A.3, lines 56–59): here the ellipsis denotes the forces (2.2) from the inter-atomic Lennard-Jones potential,

$$\frac{d\boldsymbol{q}_j}{dt} = \cdots + \begin{cases} \dfrac{K\mu}{2h^2 T_r}(T_{\text{int},+} - T_r)\boldsymbol{q}_j, & j \in \text{right action}, \\ \dfrac{K\mu}{2h^2 T_l}(T_{\text{int},-} - T_l)\boldsymbol{q}_j, & j \in \text{left action}, \\ 0, & \text{otherwise}, \end{cases} \tag{3.6}$$

where the nondimensional parameter μ is the strength of the control. Consequently, when the atoms in an action region are too cool, below $T_{\text{int},\pm}$, then the control accelerates the atoms to heat them up and vice versa.

Figure 5 demonstrates that the proportional controller is effective. The simulation is of 343 atoms in a patch of size $7 \times 7 \times 7$, coupled to boundaries at $x = \pm 7$ with specified temperatures $T_L = 0.5$ and $T_R = 1.5$. The control strength $\mu = 30$ in (3.6). Two time scales are apparent.

- On a microscopic time scale of $\Delta t < 1$ the control establishes that the temperatures in the action region differ according to the local gradient of macroscale temperature. This microtime is the time required to "lift" the given initial configuration of atoms to be in quasi-equilibrium with the macroscale field.
  In this realization, the temperature gradient is $1/(2H) = 1/14$, so that over the distance $2/7$ between mid-action regions a temperature difference of 0.25 is maintained as shown by Figure 5(b). The atomistic fluctuations about this mean increase in time as the overall temperature increases (Figure 5(a)).
  In this simple pilot scenario, with prescribed constant boundary temperatures, the desired temperature gradient across the core of the patch is constant in time. This constancy here is a consequence of the macroscale parabolic interpolation resulting in a centred difference estimate for the gradient about the symmetrically placed core. With dynamic boundary values, or asymmetry in the geometry, the desired temperature gradient across the core would generally vary in time.

https://doi.org/10.1017/S1446181117000396 Published online by Cambridge University Press

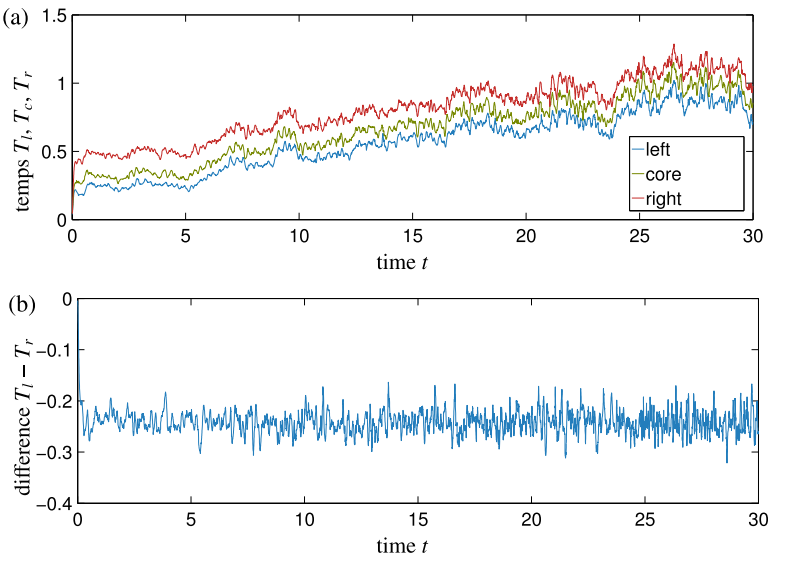

FIGURE 5. (a) Temperatures over macroscale times in the subpatch regions and (b) the temperature difference $T_l - T_r$. Simulate 343 atoms in a patch of spatial periodicity $2h = 7$ and with control strength $\mu = 30$ to couple with macroscale boundary temperatures $T_R = 1.5$ and $T_L = 0.5$ at $x = \pm 7$.

- Figure 5(a) shows that over a macroscopic time scale of $\Delta t \approx 30$ the core temperature evolves towards the correct mean of 1.0—albeit with fluctuations arising from the stochastic nature of the atomistic dynamics. This macroscopic time scale is the diffusion time for heat across the macroscopic length scale $2H = 14$. Indeed, it is on this and longer macroscopic time scales that in future developments we would implement projective integration in time [15, 21].

For completeness, we should perhaps also implement proportional controllers for the other macroscale variables of density, pressure, and average velocity. However, here there is little to control in these variables as, through conservation in the code of atoms and overall momentum, in the patch the density is constant, and the average velocity zero from the initial conditions. Thus, in this first study, we just control the nontrivial dynamics of the temperature.

Potentially, the macroscale boundary conditions at $x = \pm H$ could be fixed flux (perhaps insulated) or Robin. In such cases, we conjecture that one would simply change the macroscale parabolic interpolation (3.3) to satisfy the given macroscale boundary conditions, and that the core average matches that of the patch simulation. This issue remains for future research.

4. Analyse optimal control for a single patch

This section analyses heat diffusion PDEs that model the controlled patch atomistic simulation of Section 3. We find that a good control has strength parameter of roughly $\mu \approx 30$ in this scenario.

https://doi.org/10.1017/S1446181117000396 Published online by Cambridge University Press

We compare the patch atomistic simulation with the dynamics of the well-established continuum heat diffusion PDE (3.1) on the macroscale domain. With constant boundary temperatures, its equilibrium solution is the linear field $T = (T_R + T_L)/2 + x(T_R - T_L)/(2H)$. The dynamics superimposed on this equilibrium is an arbitrary linear combination of the modes $e^{-\lambda_n t}\sin[k_n(x+H)]$ for eigenvalues $\lambda_n = -Kk_n^2$ and wavenumbers $k_n = n\pi/(2H)$. With only one patch in the domain (Figure 3), the patch atomistic simulation can only approximate the gravest $n = 1$ mode $e^{-\lambda_1 t}\cos(k_1 x)$ with wavenumber $k_1 = \pi/(2H)$ and rate $\lambda_1 = -Kk_1^2 = -K\pi^2/(4H^2)$. We aim for the predictions (Section 3) of the single-patch scheme to match this gravest mode.

The atomistic simulation within a patch will also be reasonably well modelled by the continuum heat diffusion PDE albeit with significant microscale fluctuations. In the microscale patch scheme, Figure 3, the problem is homogeneous in the cross-sectional variables y and z, so we only explore the xt-structure, $T(x,t)$. The continuum PDE for the controlled patch is then

$$\frac{\partial T}{\partial t} = K\frac{\partial^2 T}{\partial x^2} + \frac{K\mu}{h^2}g(x,T), \quad 2h\text{-periodic in } x, \tag{4.1}$$

where the control shape, piecewise constant, is

$$g(x,T) = \begin{cases} T_{\text{int},+} - \dfrac{2}{h}\displaystyle\int_{h/4}^{3h/4} T\,dx, & h/4 < x < 3h/4, \\ T_{\text{int},-} - \dfrac{2}{h}\displaystyle\int_{-3h/4}^{-h/4} T\,dx, & -3h/4 < x < -h/4, \\ 0, & \text{otherwise.} \end{cases} \tag{4.2}$$

The temperatures $T_{\text{int},\pm}$, computed by (3.5), come from the macroscale coupling, which is the parabolic interpolation (3.3)–(3.4) via the core average $T_c = (2/h)\int_{-h/4}^{h/4} T\,dx$ to T_R and T_L at boundaries $x = \pm H$.

In the case of constant boundary temperatures, this controlled patch problem has equilibrium, with $T_c = T_0 = (T_L + T_R)/2$, of

$$T = \begin{cases} T_0 + \dfrac{\mu\,\Delta T}{4}x/h, & |x| < h/4, \\ T_0 + \dfrac{\mu\,\Delta T}{16}\left[\dfrac{3}{2} - 2(2x/h-1)^2\right]\operatorname{sgn} x, & h/4 < |x| < 3h/4, \\ T_0 + \dfrac{\mu\,\Delta T}{4}(\operatorname{sgn} x - x/h), & |x| > 3h/4, \end{cases}$$

where $\Delta T = (T_R - T_L)h/[4H(1+\mu/12)]$. A first important check is that this equilibrium has the correct mean core temperature of $T_0 = (T_R + T_L)/2$.

To understand the dynamics of the patch scheme (4.1)–(4.2), we characterize the general dynamics, relative to the equilibrium, in terms of spatial eigenfunctions. We express the dynamic analysis in terms of the half-width of the patch, h, and the ratio

https://doi.org/10.1017/S1446181117000396 Published online by Cambridge University Press

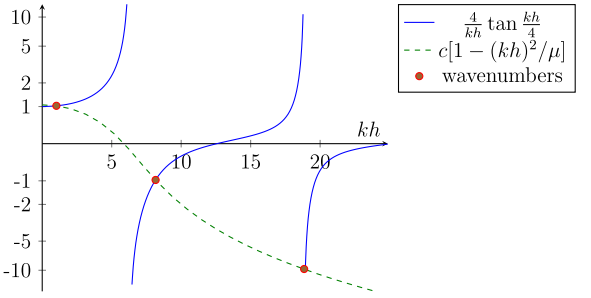

FIGURE 6. (Blue) $(4/kh)\tan(kh/4)$ has an infinite number of vertical asymptotes at $kh = 2n\pi$ for odd n; (green) the parabola $c[1-(kh)^2/\mu]$ intersects it infinitely often (here for $\mu = 34.67$ and $r = 0.64$). The vertical axis is nonlinearly scaled.

$r = h/H$, which is the fraction of macroscale space on which the microscale patch simulation is executed/solved. There are two classes of eigenfunctions: symmetric and antisymmetric within the patch.

- Symmetric eigenfunctions corresponding to temporal decay e^{-Kk^2t}, $k > 0$, are of the form

$$T = \begin{cases} A\cos kx, & |x| < h/4, \\ C + D\cos\left[k\left(x \mp \frac{h}{2}\right)\right] \pm E\sin\left[k\left(x \mp \frac{h}{2}\right)\right], & \pm h/4 \lesseqgtr x \lesseqgtr \pm 3h/4, \\ B\cos[k(x \mp h)], & x \gtrless \pm 3h/4. \end{cases}$$

  Substitute these eigenfunctions into the governing equations (3.4)–(3.5) and (4.1)–(4.2). Then straightforward algebra, detailed by Alotaibi [1, Section 2.4.2], leads to requiring the characteristic equation

$$\cos\frac{kh}{2}\sin\frac{kh}{4}\left[\left(\frac{1-7r^2/48}{1-r^2/48}\right)\frac{4}{kh}\sin\frac{kh}{4} + \left(\frac{1}{\mu}k^2h^2 - 1\right)\cos\frac{kh}{4}\right] = 0.$$

  The first factor being zero gives $kh/2 = n\pi/2$ for odd n, that is, wavenumber $k = n\pi/h$ for odd n. The second factor being zero gives $kh/4 = n\pi$ for integer n, that is, wavenumber $k = 4n\pi/h$ for integer n. The third factor being zero rearranges to

$$\frac{4}{kh}\tan\frac{kh}{4} = \left(\frac{1-r^2/48}{1-7r^2/48}\right)\left[1 - \frac{1}{\mu}(kh)^2\right]. \tag{4.3}$$

  Figure 6 plots the two sides of this equation illustrating that there are an infinite number of wavenumbers k, only one of which is small. It is this small wavenumber mode that is of macroscale interest.

https://doi.org/10.1017/S1446181117000396 Published online by Cambridge University Press

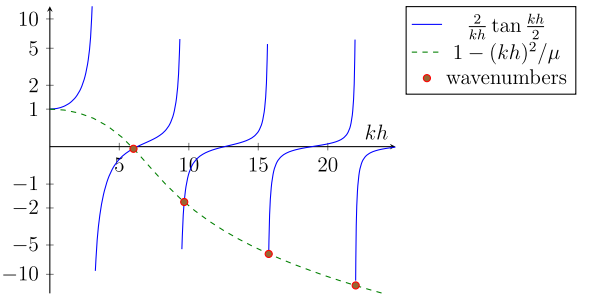

FIGURE 7. (Blue) $(2/kh)\tan(kh/2)$ has an infinite number of vertical asymptotes at $kh = n\pi$ for odd n; (green) the parabola $1-(kh)^2/\mu$ intersects it infinitely often (here for $\mu = 34.67$ and $r = 0.64$). The vertical axis is nonlinearly scaled.

- Antisymmetric eigenfunctions are of the form

$$T = \begin{cases} A\sin kx, & |x| < h/4, \\ \pm C + D\sin\left[k\left(x \mp \frac{h}{2}\right)\right] \pm E\cos\left[k\left(x \mp \frac{h}{2}\right)\right], & \pm h/4 \lesseqgtr x \lesseqgtr \pm 3h/4, \\ B\sin[k(x \mp h)], & x \gtrless \pm 3h/4. \end{cases}$$

  Substituting into the governing equations and straightforward algebra, detailed by Alotaibi [1, Section 2.4.3], leads to requiring the characteristic equation

$$\sin\frac{kh}{2}\left[\frac{2}{kh}\sin\frac{kh}{2} + \left(\frac{1}{\mu}k^2h^2 - 1\right)\cos\frac{kh}{2}\right] = 0.$$

  The first factor being zero gives $kh/2 = n\pi$ for integer n, that is, wavenumber $k = 2n\pi/h$ for integer n. The second factor being zero rearranges to

$$\frac{2}{kh}\tan\frac{kh}{2} = 1 - \frac{1}{\mu}(kh)^2.$$

  Figure 7 plots the two sides of this equation illustrating that there are an infinite number of possible wavenumbers $k > 0$ (the algebraic formula degenerates at $k = 0$, so that apparent intersection is not a possible wavenumber).

With one exception, all of these possible wavenumbers $k \propto 1/h$, and the corresponding decay rate $\propto K/h^2$ characterizes microscale modes within the patch. All these microscale modes cause the spatial structure internal in the patch to rapidly approach a quasi-equilibrium, in a time proportional to a cross-patch diffusion time of h^2/K.

The one exceptional mode corresponds to the small wavenumber k shown in Figure 6. A straightforward small-kh approximation to the left-hand side of (4.3) [1, Section 2.5] leads to

$$\left(\frac{kh}{4}\right)^2 \approx \frac{3r^2/8}{(1 - 7r^2/48) + (1 - r^2/48)48/\mu}.$$

https://doi.org/10.1017/S1446181117000396 Published online by Cambridge University Press

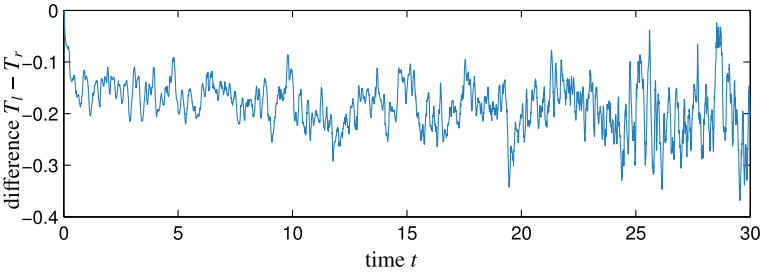

FIGURE 8. The temperature difference $T_l - T_r$. The simulation is of 343 atoms in a patch of spatial periodicity $2h = 7$ and with control strength $\mu = 3$ to couple with macroscale boundary temperatures $T_R = 1.5$ and $T_L = 0.5$ at $x = \pm 7$.

Consequently, $kh \propto r$. But the neglected terms in this approximation are $O((kh)^4)$, which are equivalently $O(r^4)$, and so for consistency the $O(r^2)$ terms in the denominator should be neglected to lead to

$$kH = kh/r \approx \sqrt{\frac{6}{1 + 48/\mu}}. \tag{4.4}$$

This wavenumber $\propto 1/H$ is characteristic of a macroscale mode, and the corresponding decay rate $\propto K/H^2$ also characterizes a single macroscale mode across the domain. For the controlled patch simulation to best predict the correct macroscale dynamics of this mode, we need the wavenumber (4.4) to match the gravest wavenumber of the heat PDE (3.1) on the macroscale domain: the start of this section found it to be $k_1 H = \pi/2$. Thus, best predictions, via a little algebra, suggest

$$\frac{1}{\mu} \approx \frac{24/\pi^2 - 1}{48} = 0.02983, \quad \text{that is, } \mu \approx 33.53 \tag{4.5}$$

for the control strength.

In an application, the result (4.5) requires an estimate of the diffusivity K. Simulations can give a rough estimate of diffusivity K for any microscale system that is diffusive-like on the microscale. Figure 8 is for the same scenario as Figure 5, but with a weaker control strength of $\mu = 3$. Figure 8 suggests that the microscale transients decay on a time scale of roughly one (and then evolve slowly on a macroscale time). That is, the leading antisymmetric microscale wavenumber k_3 is such that $Kk_3^2 \approx 1$, that is, $K \approx 1/k_3^2$. Figure 7 illustrates that $\pi < k_3 h < 2\pi$, depending upon the control via $1/\mu$. Assuming that $k_3 \ell \approx 3\pi/2$—mid-range should be good enough for rough estimates—then the microscale diffusion constant $K \approx 4h^2/(9\pi^2)$. The simulations of Figures 5 and 8 were in a patch of nondimensional length $2h = 7$ and hence here the nondimensional diffusion constant is $K \approx 0.5$, roughly. This resultant control is roughly what we found convenient for generating Figures 5 and 8. The importance of this paragraph is that it illustrates how a little analysis and a few simulations can determine a reasonably good control of the microscale periodic patch.

https://doi.org/10.1017/S1446181117000396 Published online by Cambridge University Press

5. Couple multiple periodic patches in general

The aim of this section is to establish a basis for theoretical support of the controlled patch/gap-tooth scheme for general molecular/particle/agent-based simulations. Consider the class of systems whose mesoscale dynamics is modelled by a field $u(x,t)$ governed by the stochastic reaction–advection–diffusion PDE

$$\frac{\partial u}{\partial t} = \mathcal{L}u + \alpha f(u,u_x) + \sigma g(u,u_x)\dot{W}(x,t). \tag{5.1}$$

This stochastic PDE (SPDE) (5.1) is termed "mesoscale", because it codifies the in-principle closure of some atomistic simulation on length–time scales large enough for a reasonable closure to exist (even when unknown), but smaller than the macroscale of interest, and small enough so that chaotic atomistic fluctuations may appear as "white noise" $\dot{W}$ of strength σ. The functions f and g are some functions for the closure of this mesoscale model. The closure functions f and g need not be known for our theoretical support to apply, but we do assume that f and g are smooth enough. Here we focus attention to systems where the linear operator $\mathcal{L}$ satisfies three properties:

- when u is constant, $\mathcal{L}u = 0$;
- $\mathcal{L}$ is otherwise dissipative on the mesoscale–macroscale, such as the diffusion $\mathcal{L} \approx K\partial_{xx}$;
- but where $\mathcal{L}$ is bounded due to "cut-offs" on the microscale.

This section invokes stochastic centre manifold theory (as initially developed by Boxler [4]) to provide novel support for the contention that controlled patches of the SPDE (5.1) successfully simulate its macroscale dynamics. Consequently, for a wide range of microscale simulators the same control of periodic patches will economically predict the macroscale dynamics.

This section does not precisely prescribe all restrictions on the form of the SPDE (5.1) because the aim of this section is to scope the domain and feasibility of the controlled periodic-patch scheme. The issue of whether specific systems satisfy the precise requirements for rigorous support is left for future researchers to certify for the systems of their interest.

5.1. Macroscale existence and emergence theory Figure 9 illustrates a typical scenario. Suppose that we are interested in the dynamics of the field u on a relatively large spatial domain $\mathbb{X} = [0, L]$. The patch scheme distributes M patches, equi-spaced with macroscale spacing H, and centred at $X_j = jH$. The microscale patches are $2h$-periodic with relatively small half-size h: the scale ratio $r = h/H$ would be small for efficient simulation. Let the $2h$-periodic field in the jth patch be denoted by $u_j(x,t)$ for $|x - X_j| < h$—distinct from the field $u(x,t)$ satisfying the SPDE (5.1) over all $\mathbb{X}$.

The prime quantity of interest in the macroscale simulation is a measure of the field in each patch. Measure the overall field in the jth patch by the average over the jth core region $|x - X_j| < h/4$:

$$U_j(t) := \frac{2}{h}\int_{X_j-h/4}^{X_j+h/4} u_j(x,t)\,dx, \quad j = 1,\dots,M. \tag{5.2}$$

https://doi.org/10.1017/S1446181117000396 Published online by Cambridge University Press

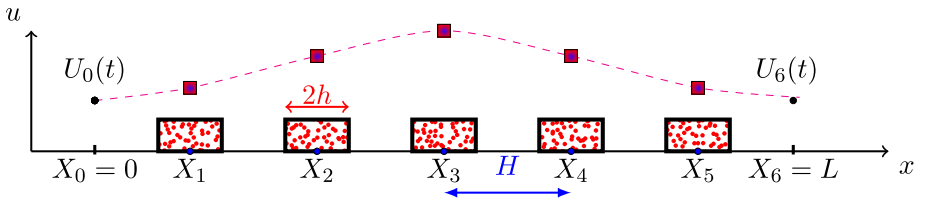

FIGURE 9. Schematic illustration of five microscale patches, $2h$-periodic, centred at $X_j = jH$, inside a macroscale domain $[0, L]$. The field $u(x,t)$, satisfying the SPDE (5.1), has some macroscale boundary conditions such as the Dirichlet conditions that $u(0,t) = U_0(t)$ and $u(L,t) = U_6(t)$.

With M patches, at the boundaries $x = 0, L$ the specified Dirichlet boundary values have synonyms $U_0(t)$ and $U_{M+1}(t)$. Let the collected core averages be denoted by the vector $\boldsymbol{U} = (U_1, U_2, \ldots, U_M)$.

Control each periodic patch via some coupling with neighbouring patches. Suppose that the simulation in each patch has an imposed proportional controller so the resultant effective system in the patches, $|x - X_j| < h$, modifies the effective SPDE (5.1) to

$$\begin{aligned}\frac{\partial u_j}{\partial t} &= \mathcal{L}u_j + \alpha f(u_j, u_{jx}) + \sigma g(u_j, u_{jx})\dot{W}_j(x,t)\\ &\quad + \mu\{[I_j^+(\boldsymbol{U},\gamma) - u_j^+]\chi_j^+(x) + [I_j^-(\boldsymbol{U},\gamma) - u_j^-]\chi_j^-(x)\}. \end{aligned} \tag{5.3}$$

The strength of the control is parametrized by μ, and is applied in the left and right action regions of each patch as coded by the indicator functions

$$\chi_j^{\pm}(x) = \begin{cases} 1, & h/4 < \pm(x - X_j) < 3h/4,\\ 0, & \text{otherwise.}\end{cases}$$

The control depends upon the difference between an interpolation, $I_j^{\pm}(\boldsymbol{U},\gamma)$, of the core averages in neighbouring patches and the local averages of the patch field in the left and right action regions,

$$u_j^{\pm}(t) = \frac{2}{h}\int_{X_j-h}^{X_j+h} u_j(x,t)\chi_j^{\pm}(x)\,dx.$$

Because Lagrange interpolation is known to produce systematic consistency in simpler scenarios [30, 31], to date we have coupled periodic patches via the Lagrange interpolation of $\boldsymbol{U}$ to estimate the macroscale field U at the mid-action points $x = X_j \pm h/2$:

$$\begin{aligned} I_j^{\pm} &= \{1 + \gamma[\pm\tfrac{1}{2}r\bar{\mu}\delta + \tfrac{1}{8}r^2\delta^2]\\ &\quad + \gamma^2[\mp r(\tfrac{1}{4} - \tfrac{1}{8}r)\bar{\mu}\delta^3 - r(\tfrac{1}{8} - \tfrac{1}{16}r)\delta^4] + \cdots\}U_j, \end{aligned} \tag{5.4}$$

expressed in terms of centred difference and mean operators $\delta U_j = U_{j+1/2} - U_{j-1/2}$ and $\bar{\mu}U_j = (U_{j+1/2} + U_{j-1/2})/2$. The coupling parameter γ is an artificial homotopy parameter that empowers us to connect a theoretical base at $\gamma = 0$ to the fully coupled

https://doi.org/10.1017/S1446181117000396 Published online by Cambridge University Press

case $\gamma = 1$ which is of interest. That is, this embeds the relevant physical problem, at $\gamma = 1$, into a family of problems parametrized by γ. For the theory of this section we require three things of the dependency of the interpolation operator $I_j^{\pm}$ on the parameter γ: $I_j^{\pm}(\boldsymbol{U}, \gamma)$ be smooth; $I_j^{\pm}(\boldsymbol{U}, 0) = U_j$; and $I_j^{\pm}(\boldsymbol{U}, 1)$ corresponds to the coded coupling of the computational patch scheme. Further, although not necessary, it is convenient to express $I_j^{\pm}(\boldsymbol{U}, \gamma)$ as a polynomial in γ, as in (5.4), such that a truncation which neglects terms $O(\gamma^{p+1})$ invokes an $I_j^{\pm}$ which depends upon only $U_{j-p}, \dots, U_{j+p}$. This property then empowers convenient comparison with classic finite differences/elements.

Theoretical support is based upon an equilibrium of the controlled patch system (5.3). For parameters $\alpha = \sigma = \gamma = 0$, the system (5.3) is linear with $u_j(x, t) =$ constant being equilibria. Being independently constant in each of the M patches, these equilibria form an M-dimensional subspace $\mathbb{E}_0$ (a subspace of the space of $(\alpha, \sigma, \gamma, u_1(x), u_2(x), \dots, u_M(x))$). By the definition (5.2) of the core averages, we write these equilibria as the patch field $u_j(x, t) = U_j$ such that $dU_j/dt = 0$ for $j = 1, \dots, M$.

This subspace commonly and usefully persists upon perturbation. Specifically, we are interested in perturbations by nonlinearity (nonzero α), by stochasticity (nonzero σ), and most importantly by coupling with neighbouring patches (nonzero γ). Consider the dynamics of the controlled patches, SPDE (5.3), linearized about each of the equilibria in $\mathbb{E}_0$, namely, for patch field u_j being $2h$-periodic,

$$\frac{\partial u_j}{\partial t} = \mathcal{L}u_j + \mu[\{U_j - u_j^+\}\chi_j^+(x) + \{U_j - u_j^-\}\chi_j^-(x)]. \tag{5.5}$$

As for diffusion, $\mathcal{L} = K\partial_{xx}$, we assume that the operator on the right-hand side of (5.5) has spectrum $0 = \lambda_1 > -\beta > \Re\lambda_2 \geq \Re\lambda_3 \geq \cdots$, where the size, β, of the spectral gap depends upon the size of the patches. In the linearization (5.5), each of the M patches are isolated from each other and consequently all of these eigenvalues have multiplicity M (at least). For example, in the case of mesoscale diffusion, $\mathcal{L} = K\partial_{xx}$, the analysis of Section 4 applies except with the replacement of the factor $(1 - 7r^2/48)/(1 - r^2/48)$ by simply one: consequently, Section 4 establishes that here $\lambda_1 = 0$, $\lambda_2 = -K\pi^2/h^2$, and so on, and consequently we may choose bound $\beta = 9K/h^2$, say. There are three extra zero eigenvalues, one each for the parameters α, σ, and γ, corresponding to the extended state space formed by adjoining $d\alpha/dt = d\sigma/dt = d\gamma/dt = 0$. In this scenario, and subject to some technical caveats on the nature of the functions $f(u, u_x)$ and $g(u, u_x)\dot{W}(x, t)$, the marvellous theory of Aulbach and Wanner [2] applies to establish that there exists an $(M + 3)$-dimensional slow manifold to the controlled patch mesoscale system (5.3) (or $(mM + 3)$-dimensional, when the zero eigenvalue of (5.5) has multiplicity m within each patch). The slow manifold exists globally in $\boldsymbol{U}$ and in a finite domain about zero in the parameters (α, σ, γ).

Although mesoscale diffusion $K\partial_{xx}$ is strictly an unbounded operator, such a diffusive operator is only a long-wavelength approximation to the microscale dynamics, which usually has a bounded equivalent operator (for example, difference operators on a lattice). Hence, the simulation $\mathcal{L}$ is usually bounded as required by Aulbach and Wanner [2]. The global existence explicitly proved by Aulbach and Wanner [2] also requires perturbations to be Lipschitz and bounded, whereas here

https://doi.org/10.1017/S1446181117000396 Published online by Cambridge University Press

the inter-patch coupling as posited is unbounded: consequently, here we establish theoretical support in a finite local domain instead of the global domain.

Further, the theory establishes that the slow manifold emerges exponentially quickly from all initial conditions in some finite domain about the slow manifold [2, Section 4]. More specifically, the exponential transients are $O(e^{-\beta t})$ as $t \to \infty$. These transients are all microscale subpatch modes as they correspond to the dissipative modes within isolated patches. For example, in the diffusive case the lower bound $\beta = 9K/h^2$ on the decay rate corresponds to an intra-patch diffusion time which is very small for the useful case of small patches. Just as for the single-patch case of Section 4, this leaves the slow manifold and the evolution thereon to be the emergent macroscale dynamics of the controlled periodic-patch scheme.

5.2. Constructing a slow manifold predicts the macroscale To confirm, or otherwise, that the patch scheme's macroscale dynamics matches that of the simulation, we have to construct the slow manifold and its evolution and compare with the mesoscale SPDE (5.1). Because the details of the slow-manifold construction are closely linked to the details of the underlying system, here we specifically address the class of systems whose mesoscale has the diffusive $\mathcal{L} = K\partial_{xx}$. Further, noise from microscale chaos enormously complicates the construction [6, 28], so here we further restrict analysis to the cases with $\sigma = 0$.

A good robust method to construct slow manifolds is an iteration based upon the residuals of the governing equations [27, 29, Part V]; successive approximations to the slow manifold are corrected until the residuals are zero to within a pre-specified order of error. The algebraic machinations of the construction are involved and of little interest, so are not recorded here. Instead we comment on two aspects:

- computer algebra readily constructs a slow-manifold model of the macroscopic dynamics of the controlled periodic-patch scheme (supplementary material, Appendix B) for a variety of systems in the class (5.1);
- as an example, we show that the controlled periodic-patch scheme applied to an advection–diffusion reasonably approximates the correct macroscale advection–diffusion.

For example, consider a microscale simulation whose mesoscale is the linear advection–diffusion PDE

$$u_t = Ku_{xx} - \alpha u_x, \tag{5.6}$$

with macroscale boundary conditions of (MH)-periodicity so that by symmetry each controlled patch is identical. Computer algebra, detailed in the supplementary material (Appendix B), constructs the slow manifold of the corresponding controlled periodic-patch system (5.3). As the simplest example, with no advection, $\alpha = 0$, three iterations find that each subpatch field is piecewise parabolic: in terms of $\xi = (x - X_j)/h$ the jth

https://doi.org/10.1017/S1446181117000396 Published online by Cambridge University Press

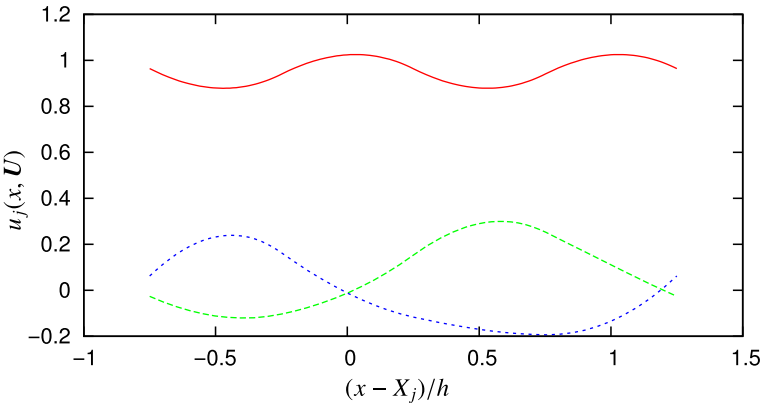

FIGURE 10. Subpatch periodic field $u_j(\xi, \boldsymbol{U})$ for amplitudes $\boldsymbol{U} = \boldsymbol{0}$ except for: red-solid, $U_j = 1$; green-dashed, $U_{j+1} = 1$; blue-dotted, $U_{j-1} = 1$. For illustrative purposes this case is for $r = h = H = 1$, $\mathcal{L} = \partial_{xx}$, advection $\alpha = 1$, and control $\mu = 30$. Consequently the patch core is $|x - X_j|/h < 1/4$ and action regions are $1/4 < |x - X_j|/h < 3/4$.

patch field

$$u_j = U_j + \gamma\Big[U_j \frac{r^2 - 48\xi^2}{16(1 + 48/\mu)} + \sum_{\pm} U_{j\pm1} \frac{-r^2 \pm 24\xi + 48\xi^2 + 12(-r^2 \pm 96\xi + 48\xi^2)/\mu}{32(1 + 48/\mu)(1 + 12/\mu)}\Big] + O(\gamma^2),$$

in the core $|\xi| < 1/4$, and somewhat longer expressions in the other regions. Figure 10 plots leading order shapes of the fields in a patch across all four regions in the case of advection $\alpha = 1$: the general field in the patch is the linear combination of these curves with coefficients of U_j and $U_{j\pm1}$. This example is just a specific case of the reasonably general construction of the macroscale slow manifold. The small asymmetry in Figure 10 is due to the advection at velocity $\alpha = 1$ in this case. The downward curvature of the red-solid curve in the core region, $|\xi| < 1/4$, and the back/buffer region, is due to the out-of-equilibrium macroscopic decay in the jth patch when surrounded by patches with zero core average, $U_{j\pm1} = 0$. However, the interest on the macroscale is not the detailed subpatch fields, but the long-term evolution of the macroscale amplitudes $\boldsymbol{U}$.

The macroscale amplitudes evolve according to the dynamics on the slow manifold. Simultaneous with constructing the shape of the slow manifold, the computer algebra (supplementary material, Appendix B) also finds the evolution of $\boldsymbol{U}$ on the slow manifold as a system of coupled ODEs. For the general advection–diffusion mesoscale PDE (5.6) the evolution on the slow manifold is

$$\frac{dU_j}{dt} = -\gamma\alpha \frac{15(U_{j+1} - U_{j-1})}{8H(1 + 48/\mu)(1 + 12/\mu)} + \gamma K \frac{3(U_{j-1} - 2U_j + U_{j+1})}{H^2(1 + 48/\mu)} + O(\gamma^2, \alpha^2).$$

https://doi.org/10.1017/S1446181117000396 Published online by Cambridge University Press

Evaluating at full coupling $\gamma = 1$, this slow-manifold analysis then predicts that the emergent macroscale dynamics of the controlled periodic patches of advection–diffusion (5.6) is

$$\frac{dU_j}{dt} \approx -\alpha \frac{15(U_{j+1} - U_{j-1})}{8H(1 + 48/\mu)(1 + 12/\mu)} + K \frac{3(U_{j-1} - 2U_j + U_{j+1})}{H^2(1 + 48/\mu)}. \tag{5.7}$$

Via such a model, the theory of this section empowers us to predict what the controlled periodic-patch scheme would do for a range of mesoscale systems.

In this particular example of general advection–diffusion, we use the predicted model (5.7) to now identify a good control strength in the periodic-patch scheme. The macroscale discrete system (5.7) has equivalent PDE

$$U_t = -\alpha \frac{15}{4(1 + 48/\mu)(1 + 12/\mu)} U_x + K \frac{3}{1 + 48/\mu} U_{xx} + O(H^2).$$

Thus, the effective advection of the periodic-patch scheme will equal that of the posed underlying mesoscale system (5.6) when the control strength is chosen such that

$$\frac{15}{4H(1 + 48/\mu)(1 + 12/\mu)} = 1, \quad \text{that is, } \mu \approx \frac{120 + 24\sqrt{69}}{11} = 29.0326.$$

Similarly, the effective diffusion will equal that of the posed underlying mesoscale system (5.6) when

$$\frac{3}{1 + 48/\mu} \approx 1, \quad \text{that is, } \mu \approx 24.$$

To this level of approximation there may not be a single best control strength. Nonetheless, the closeness of these two good control strengths is encouraging for applications of the controlled periodic-patch scheme. Systematic exploration to higher order, and with other controller schemes, would give more accurate predictions for such optimal control in a wider range of mesoscale systems.

A future extension to a wider range of mesoscale systems is important, because the primary rationale for the equation-free methodology is that its main application is to systems for which we do not know a meso–macro-scale closure. Hence, we need to develop control schemes useful for a wide range of systems such as the class (5.1).

6. Conclusion

The atomistic simulation described by Section 2 is just one important example of microscale simulators used widely in engineering and science. In particular, we address the class of simulators that are given with periodic conditions on the microscale. The challenge is to create a wrapper around such microscale periodic simulators in order to effectively predict macroscale behaviour. Section 3 implemented a proportional controller applied to action regions in the patch to couple patches to its neighbours over unsimulated space.

Analysis of atomistic simulations based upon just one small patch, and the corresponding controlled diffusion PDE in Section 4, indicates that there are good

https://doi.org/10.1017/S1446181117000396 Published online by Cambridge University Press

values for the control strength. Section 5 then created a theoretical basis for certifying that the emergent behaviour of many coupled, controlled, periodic patches does indeed predict appropriate macroscale, system-level dynamics for a wide range of microscale simulators.

The construction of a slow-manifold model for the equation-free patch scheme provides an innovative route to explore algebraically how best to couple such periodic patches. Here Section 5.2 established the algebraic analysis to be feasible. Further research could search for optimal core and action region sizes, optimal weight functions for the averages in the regions, refine the interpolation that couples the patches, and be applied to other controllers.

Acknowledgements

Parts of this work were supported by the Taif University in Saudi Arabia and by grant DP150102385 from the Australian Research Council. We thank Yannis Kevrekidis for many useful discussions and support.

Supplementary material

Supplementary material is available at doi:10.1017/S1446181117000396.

References

[1] H. Alotaibi, "Developing multiscale methodologies for computational fluid mechanics", Ph. D. Thesis, School of Mathematical Sciences, University of Adelaide, 2017.

[2] B. Aulbach and T. Wanner, "The Hartman–Grobman theorem for Caratheodory-type differential equations in Banach spaces", *Nonlinear Anal.* **40** (2000) 91–104; doi:10.1016/S0362-546X(00)85006-3.

[3] J. Bechhoefer, "Feedback for physicists: a tutorial essay on control", *Rev. Modern Phys.* **77** (2005) 783–836; doi:10.1103/RevModPhys.77.783.

[4] P. Boxler, "A stochastic version of the centre manifold theorem", *Probab. Theory Related Fields* **83** (1989) 509–545; doi:10.1007/BF01845701.

[5] J. E. Bunder and A. J. Roberts, "Patch dynamics for macroscale modelling in one dimension", in: *Proc. 10th Biennial Engineering Mathematics and Applications Conf., EMAC-2011* (eds M. Nelson et al.), *ANZIAM J.* **53** (2012) C280–C295; doi:10.21914/anziamj.v53i0.5074.

[6] J. E. Bunder and A. J. Roberts, "Resolution of subgrid microscale interactions enhances the discretisation of nonautonomous partial differential equations", *Appl. Math. Comput.* **304** (2017) 164–179; doi:10.1016/j.amc.2017.01.056.

[7] J. E. Bunder, A. J. Roberts and I. G. Kevrekidis, "Good coupling for the multiscale patch scheme on systems with microscale heterogeneity", *J. Comput. Phys.* (2017) (in press); doi:10.1016/j.jcp.2017.02.004.

[8] M. Cao and A. J. Roberts, "Multiscale modelling couples patches of wave-like simulations", in: *Proc. 16th Biennial Computational Techniques and Applications Conf., CTAC-2012* (eds S. McCue et al.), *ANZIAM J.* **54** (2013) C153–C170; doi:10.21914/anziamj.v54i0.6137.

[9] M. Cao and A. J. Roberts, "Multiscale modelling couples patches of nonlinear wave-like simulations", *IMA J. Appl. Math.* **81** (2016) 228–254; doi:10.1093/imamat/hxv034.

[10] E. J. Carr, P. Perré and I. W. Turner, "The extended distributed microstructure model for gradient-driven transport: a two-scale model for bypassing effective parameters", *J. Comput. Phys.* **327** (2016) 810–829; doi:10.1016/j.jcp.2016.10.004.

[11] H. Cheng, L. Greengard and V. Rokhlin, "A fast adaptive multipole algorithm in three dimensions", *J. Comput. Phys.* **155** (1999) 468–498; doi:10.1006/jcph.1999.6355.
[12] M. T. Dove, "An introduction to atomistic simulation methods", *Sem. SEM* **4** (2008) 7–37; http://www.ehu.eus/sem/seminario_pdf/SEM_SEM_4_7-37.pdf.
[13] D. J. Evans and W. G. Hoover, "Flows far from equilibrium via molecular dynamics", *Annu. Rev. Fluid Mech.* **18** (1986) 243–264; doi:10.1146/annurev.fl.18.010186.001331.
[14] Y. Frederix et al., "Equation-free methods for molecular dynamics: a lifting procedure", *Proc. Appl. Meth. Mech.* **7** (2007) 20100003–20100004; doi:10.1002/pamm.200700025.
[15] C. W. Gear and I. G. Kevrekidis, "Projective methods for stiff differential equations: problems with gaps in their eigenvalue spectrum", *SIAM J. Sci. Comput.* **24** (2003) 1091–1106; doi:10.1137/S1064827501388157.
[16] D. Givon, R. Kupferman and A. Stuart, "Extracting macroscopic dynamics: model problems and algorithms", *Nonlinearity* **17** (2004) R55–R127; doi:10.1088/0951-7715/17/6/R01.
[17] E. Hairer, C. Lubich and G. Wanner, "Geometric numerical integration illustrated by the Stormer–Verlet method", *Acta Numer.* **12** (2003) 399–450; doi:10.1017/S0962492902000144.
[18] P. Hassard, I. Turner, T. Farrell and D. Lester, "Simulation of micro-scale porous flow using smoothed particle hydrodynamics", in: *Proc. 17th Biennial Computational Techniques and Applications Conf., CTAC-2014* (eds J. Sharples and J. Bunder), *ANZIAM J.* **56** (2016) C463–C480; doi:10.21914/anziamj.v56i0.9408.
[19] M. F. Horstemeyer, "Multiscale modeling: a review", in: *Practical aspects of computational chemistry* (eds J. Leszczynski and M. K. Shukla), (Springer, Dordrecht, 2009) Ch. 4, 87–135; doi:10.1007/978-90-481-2687-3_4.
[20] M. Kalweit and D. Drikakis, "Multiscale simulation strategies and mesoscale modelling of gas and liquid flows", *IMA J. Appl. Math.* **76** (2011) 661–671; doi:10.1093/imamat/hxr048.
[21] I. G. Kevrekidis and G. Samaey, "Equation-free multiscale computation: algorithms and applications", *Annu. Rev. Phys. Chem.* **60** (2009) 321–344;; doi:10.1146/annurev.physchem.59.032607.093610.
[22] J. Koplik and J. R. Banavar, "Continuum deductions from molecular hydrodynamics", *Annu. Rev. Fluid Mech.* **27** (1995) 257–292; doi:10.1146/annurev.fl.27.010195.001353.
[23] P. Koumoutsakos, "Multiscale flow simulations using particles", *Annu. Rev. Fluid Mech.* **37** (2005) 457–487; doi:10.1146/annurev.fluid.37.061903.175753.
[24] P. Liu, G. Samaey, C. W. Gear and I. G. Kevrekidis, "On the acceleration of spatially distributed agent-based computations: a patch dynamics scheme", *Appl. Numer. Math.* **92** (2015) 54–69; doi:10.1016/j.apnum.2014.12.007.
[25] J. Moller, O. Runborg, P. G. Kevrekidis, K. Lust and I. G. Kevrekidis, "Equation-free, effective computation for discrete systems: a time stepper based approach", *Internat. J. Bifur. Chaos* **15** (2005) 975–996; http://www.worldscinet.com/ijbc/15/1503/S0218127405012399.html.
[26] S. Plimpton et al., "Large-scale atomic/molecular massively parallel simulator", Technical Report, Sandia National Laboratories, Department of Energy, USA, 2016; http://lammpssandiagov.
[27] A. J. Roberts, "Low-dimensional modelling of dynamics via computer algebra", *Comput. Phys. Comm.* **100** (1997) 215–230; doi:10.1016/S0010-4655(96)00162-2.
[28] A. J. Roberts, "Resolving the multitude of microscale interactions accurately models stochastic partial differential equations", *LMS J. Comput. Math.* **9** (2006) 193–221;; doi:10.1112/S146115700000125X.
[29] A. J. Roberts, *Model emergent dynamics in complex systems* (SIAM, Philadelphia, PA, 2015); http://bookstore.siam.org/mm20/.
[30] A. J. Roberts and I. G. Kevrekidis, "General tooth boundary conditions for equation free modelling", *SIAM J. Sci. Comput.* **29** (2007) 1495–1510; doi:10.1137/060654554.
[31] A. J. Roberts, T. MacKenzie and J. Bunder, "A dynamical systems approach to simulating macroscale spatial dynamics in multiple dimensions", *J. Engrg. Math.* **86** (2014) 175–207; doi:10.1007/s10665-013-9653-6.

[32] D. Roose, E. Nies, T. Li, C. Vandekerckhove, G. Samaey and Y. Frederix, "Lifting in equation-free methods for molecular dynamics simulations of dense fuids", *Discrete Contin. Dyn. Syst. Ser. B* **11** (2009) 855–874; doi:10.3934/dcdsb.2009.11.855.

[33] G. Samaey, I. G. Kevrekidis and D. Roose, "The gap-tooth scheme for homogenization problems", *Multiscale Model. Simul.* **4** (2005) 278–306; doi:10.1137/030602046.

[34] G. Samaey, D. Roose and I. G. Kevrekidis, "Patch dynamics with buffers for homogenization problems", *J. Comput. Phys.* **213** (2006) 264–287; doi:10.1016/j.jcp.2005.08.010.

[35] G. J. Wagner et al., "Accelerated molecular dynamics and equation-free methods for simulating diffusion in solids", Technical Report SAND2011-6659, Sandia National Laboratories, Department of Energy, USA, 2011; http://www.osti.gov/scitech/biblio/1030307.

[36] H. Yoshida, "Recent progress in the theory and application of symplectic integrators", *Celestial Mech. Dynam. Astronom.* **56** (1993) 27–43; doi:10.1007/BF00699717.